BMC Oral Health

RESEARCH

Open Access

Comparative evaluation of four traction scenarios on a labially impacted dilacerated maxillary central incisor: a three-dimensional finite element analysis

Enas Senan Alyafrusee[1,2,3], Bowen Zheng[1,2*], Wael Telha[4], Mengyao Li[1,2], Haopeng Wu[1,2], Xiaofeng Yang[1,2], Bushra Sufyan Almaqrami[5,6], Naseem Ali Al-Worafi[1,2], Majedh Abdo Ali Al-Somairi[1,2,3], Maged S. Alhammadi[7] and Yi Liu[1,2*]

Abstract

Objective This study aimed to analyze the stress distribution in the dentoalveolar structures of a labially impacted dilacerated maxillary central incisor during orthodontic traction, considering different positions of the traction button on the tooth's crown through finite element analysis (FEA).

Materials and methods Four three-dimensional (3D)finite element models (FEM) were created to simulate the maxilla of a 9-year-old female patient, featuring a left labially impacted dilacerated maxillary central incisor with the only variation being the position of the orthodontic traction button: at the incisal third of the labial surface (Model A), at the incisal third of the palatal surface (Model B), at the middle third of the palatal surface (Model C), and the cervical third of the palatal surface (Model D). Material parameters, grids, boundary conditions, coordinate systems, and load conditions were set in Ansys to establish the FEM for traction of the impacted incisor. A 100 g total traction force was applied between the button and a 0.016×0.022-inch stainless steel archwire in the direction perpendicular to the impacted tooth's crown. The initial tooth displacements, biomechanical stress at the root apex, alveolar bone von Mises stress, and hydrostatic stress of the periodontal ligament (PDL) under the four conditions were analyzed and compared.

Results The impact of traction button positioning on tooth displacement, stress distribution, and bone loading was assessed in four models. Model B demonstrated the highest labiopalatal and vertical displacement. The stress concentrations in the impacted tooth's root were highest in model B, particularly in the cervical region labially, while model D showed the lowest root stress. Maximum stress in the alveolar bone was also observed in models A and B, particularly on the palatal surface near the cervical region. Hydrostatic stress in the periodontal ligament was highest in model B and lowest in model D.

*Correspondence:
Bowen Zheng
bwzheng@cmu.edu.cn
Yi Liu
liuyi@cmu.edu.cn

Full list of author information is available at the end of the article

Conclusion The traction button positioned on the incisal third of the labial or palatal surface facilitates significant tooth movement. Still, it carries a higher risk of periodontal ligament damage, root and alveolar bone resorption. In contrast, the traction button positioned on the cervical third of the palatal surface, while less effective for movement, generates the least stress.

Keywords Impacted maxillary central incisor, Dilaceration, Three-dimensional finite element analysis, Hydrostatic stress of periodontal ligament, Stress distribution

Introduction

Maxillary incisors are essential for facial aesthetics, prominently displayed during speech and smiling [1, 2]. A missing incisor can cause functional issues, such as difficulty in biting and chewing, speech problems, misalignment of teeth, and facial aesthetic problems [3]. Eruption failure typically occurs between ages 7 and 9 during the mixed dentition stage [4, 5]. The maxillary incisor is the third most commonly impacted tooth, with an incidence of 0.06–0.20%. Delayed eruption is defined if the contralateral incisor erupts 6 months earlier, lower incisors erupt more than a year earlier, or there is a deviation in the normal eruption sequence [3, 6]. Causes of eruption failure include pathological obstructions, tooth malformation, ectopic positioning, non-vital or ankylosed primary teeth, endocrine abnormalities, or bone disease. Pathological obstructions can arise from supernumerary teeth, odontomas, cysts, or tissue barriers due to early primary tooth loss [7]. Trauma to the anterior region may lead to the loss of the deciduous tooth, dilaceration, arrested root development, or intrusive luxation of the permanent incisor. Any alteration in tooth position or morphology can hinder eruption [8]. The extent of damage depends on the tooth's developmental stage, trauma type, and direction [2].

The labially impacted maxillary central incisor with dilaceration is the most complex type of impacted tooth, with its crown oriented upwards and the palatal aspect facing labially. This elevated position results in a low success rate for correction [9]. Management complications include prolonged orthodontic treatment, influenced by the tooth's position and angulation. Successful alignment depends on accurately determining the traction method and direction without damaging the dentoalveolar structures. While three-dimensional (3D) imaging can help localize the impacted tooth and guide traction direction [10], there are no clinical guidelines for the appropriate traction method.

The oral cavity is a complex biomechanical system, making internal study challenging. Therefore, utilizing computer technology for oral biomechanics offers a more intuitive approach. Finite element analysis (FEA) is a numerical technique widely applied in computer-aided engineering since the 1960s to solve complex structural equations and analyze mechanical properties in various systems, including biological contexts [11]. In FEA, structures are discretized into more minor elements, each assigned specific material properties, allowing for applying loads and boundary conditions to simulate real-world scenarios. This technique is valued for its non-invasive nature, visualization capabilities, and repeatability, making it particularly useful in biological research. In recent years, FEA has become increasingly prominent in studies of biological systems, where it is used to examine the mechanical properties of facial tissues, dental materials, and bone substitute biomaterials [11, 12]. Through this approach, researchers gain critical insights into the tension and compression forces experienced by these materials, contributing to a better understanding of their structural behavior under various conditions [13].

Previous studies have utilized FEA to analyze stress distribution in periodontal tissue during the treatment of labially impacted maxillary central incisors under various traction forces [13, 14]. However, these studies primarily focused on the overall force application and stress distribution without explicitly examining the influence of traction button positioning. Since the button position directly affects force direction and moment generation, a detailed biomechanical analysis is necessary to determine the optimal placement for effective and safe traction.

This is the first FE-based biomechanical analysis focused on the optimal traction button position for labially impacted dilacerated maxillary central incisors. Therefore, this study aims to determine the optimal traction button position for efficient and controlled tooth movement. This study used three-dimensional finite element analysis (3D FEA) to evaluate the biomechanical effects of different traction button positions on the tooth crown, analyzing key parameters such as tooth displacement, root stress, alveolar bone Von Mises stress, and periodontal ligament strain. The findings of this study would provide a valuable reference for clinical orthodontic traction, aiding in the selection of an optimal traction strategy for such cases.

Methodology

Patient selection

This study utilized cone beam computed tomography (CBCT) data of a 9-year-old female patient in the mixed dentition phase who presented with a left labially impacted dilacerated maxillary central incisor. The CBCT imaging revealed a labially impacted tooth with dilaceration and a relatively low vertical position, with the crown directed normally or slightly mesially. The patient had no history of orthodontic or restorative treatments, and there were no systemic diseases or pathological conditions in the maxillary anterior region. The patient's parents signed informed consent to participate in the study and allowed their daughter's CBCT data to be used. This study was approved by the Ethics Committee of China Medical University School, China (Approval No. CMUKQ-2024-018), and all methods were carried out in accordance with the principles of the Declaration of Helsinki.

Original 3D model design

The CBCT scans were performed using the i-CAT® CBCT system (KAVO, Germany) at the affiliated Stomatological Hospital of China Medical University, China. The imaging parameters included a 120 kV and 5 mA setting with a 23 cm × 17 cm field of view, an exposure time of 17.8 s, a voxel size of 0.3 mm, and a slice thickness of 2 mm. Continuous scans of the maxilla produced 565 slices stored in Digital Imaging and Communication in Medicine (DICOM) format, which were imported into Mimics software (version 21.0; Materialize, Belgium) for 3D reconstruction and ultimately saved in STL format. The preliminary STL model was further refined in Geomagic Studio software (version 2015; 3D Systems, USA), where the periodontal ligament (PDL) model was derived through Boolean operations. The PDL thickness ranged from 0.15 to 0.38 mm [15]. Using NX software (version 1911; Siemens, Germany), a 3D model of the maxillary arch was established. The alveolar bone's left, right, and bottom surfaces were set as fixed constraints to simulate attachment to the surrounding maxillary bone. Additionally, the bonding contact was set for interfaces of bone-PDL, PDL-tooth, tooth-attachment, and attachments-wire.

The 3D model of the maxillary arch incorporating a 0.016×0.022-inch stainless steel archwire, orthodontic braces, buccal tubes, metal chain-round button with a concave pad and gridded base (3 mm diameter of the bottom surface and 1 mm height), and a traction hook model was created. Initially, calipers were used to measure the outer dimensions of the orthodontic braces, buccal tubes, metal chain-round button, and traction hook. In the NX sketch environment, the cross-sectional outline of the orthodontic braces was drawn, and the extrude command was used to create solid models of the orthodontic braces and buccal tubes. The orthodontic braces were placed at the center of the teeth crown, and their position was finely adjusted for accurate representation. The archwire was generated within the orthodontic braces by drawing its curvature in the NX sketch. A 0.016×0.022-inch stainless steel archwire was created, with its shape adjusted according to the natural alignment of the maxillary teeth. The cross-sectional outline was sketched for the metal chain-round button, and the rotate command was applied to create a solid model. It was positioned centrally on the impacted tooth crown. The metal chain, measuring 2 mm in length and 0.5 mm in height, was vertically extended onto the traction hook, which was fixed to the archwire to connect the button and the archwire, thereby simulating the applied traction force. The traction button was modelled in four distinct positions: an incisal third of the labial surface (Model A), an incisal third of the palatal surface (Model B), the middle third of the palatal surface (Model C), and the cervical third of the palatal surface (Model D) (See Fig. 1).

Material properties and mesh creation

Table 1 summarizes the mechanical properties of the materials used in this study. All materials were set as continuous, homogeneous, isotropic linear elastic bodies [11, 12, 16–22]. The created 3D finite element model was constructed using the ANSYS Workbench software (version 2019; Ansys; USA). The geometric model included the alveolar bone, PDL, tooth, and traction button. The model was discretized into finite elements with different element sizes assigned according to the structural characteristics: alveolar bone was meshed with an element size of 2 mm, PDL was meshed with an element size of 0.5 mm, the tooth was meshed with an element size of 1 mm, and traction button was meshed with an element size of 0.25 mm.

Mesh quality was critically assessed using standard indicators: Jacobian Ratio: values range from 0 to 1, with values closer to 1 indicating minimal distortion, Aspect Ratio: an optimal value of 1 is desired; values below 20 are acceptable for structural analysis, Maximum Corner Angle: ideally around 60°; actual values are monitored to ensure acceptable element shape, and Skewness: Ranges from 0 (ideal) to 1 (highly distorted), with lower values being preferred.

A mesh convergence analysis was conducted using three different mesh configurations to ensure that the simulation results were not significantly influenced by mesh density. The key outcome parameters, such as tooth displacement and root stresswere compared across these configurations: configuration 1: employed a coarser mesh (alveolar bone at 3 mm, PDL at 1 mm, tooth at 1 mm, traction button at 0.5 mm), configuration 2: used intermediate refinement (alveolar bone at 2 mm, PDL at 0.5 mm, tooth at 1 mm, traction button at 0.25 mm), and configuration 3: utilized a finer mesh (alveolar bone at 1.5 mm, PDL at 0.2 mm, tooth at 1 mm, traction button at 0.2 mm). The results showed minimal variations in the measured tooth displacement and root stress among the three models, indicating convergence of the solution.

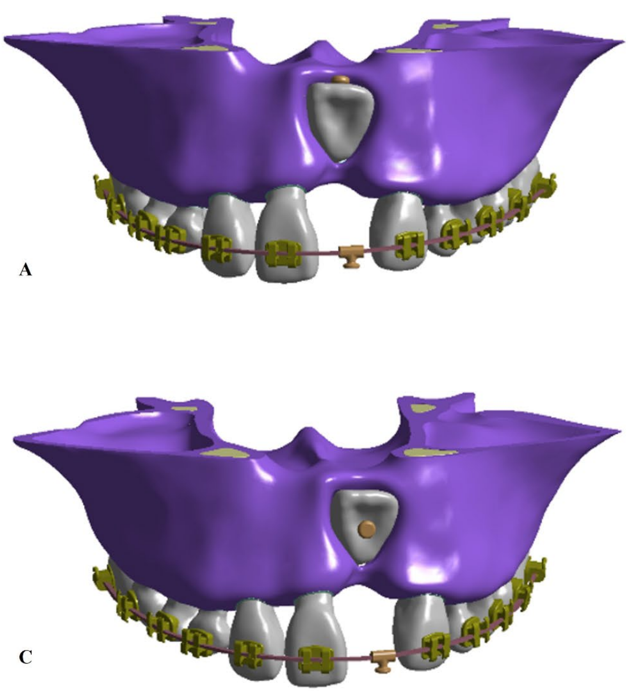

Fig. 1 The position of the traction button on the labially impacted dilacerated maxillary central incisor. **A**; on the incisal third of the labial surface, **B**; on the incisal third of the palatal surface, **C**; on the middle third of the palatal surface, and **D**; on the cervical third of the palatal surface

Table 1 Properties of the model materials

Materials	Young's modulus (MPa)	Poisson's ratio
Tooth	1.96×10^4	0.3
Cortical bone	1.37×10^4	0.26
Cancellous bone	1.37×10^3	0.3
Periodontal ligament	6.9×10^{-1}	0.45
Orthodontic wire	2×10^5	0.3
Button	1.14×10^5	0.35
Traction hook	2×10^5	0.3
Orthodontic brace	2.06×10^5	0.3
Buccal tube	2×10^5	0.3

Configuration 2 was ultimately selected as the optimal mesh configuration, balancing computational efficiency with accuracy (comprising 479,573 nodes and 267,837 elements) (Fig. 2).

Boundaries, coordinate systems, and load conditions

As illustrated in Fig. 2, in this study, fixed constraints were applied around the upper part of the maxillary bone [23], and a local coordinate system was established, Fig. 3. When setting up the coordinate system with the crown centroid as the reference point, the x-axis (mesiodistal

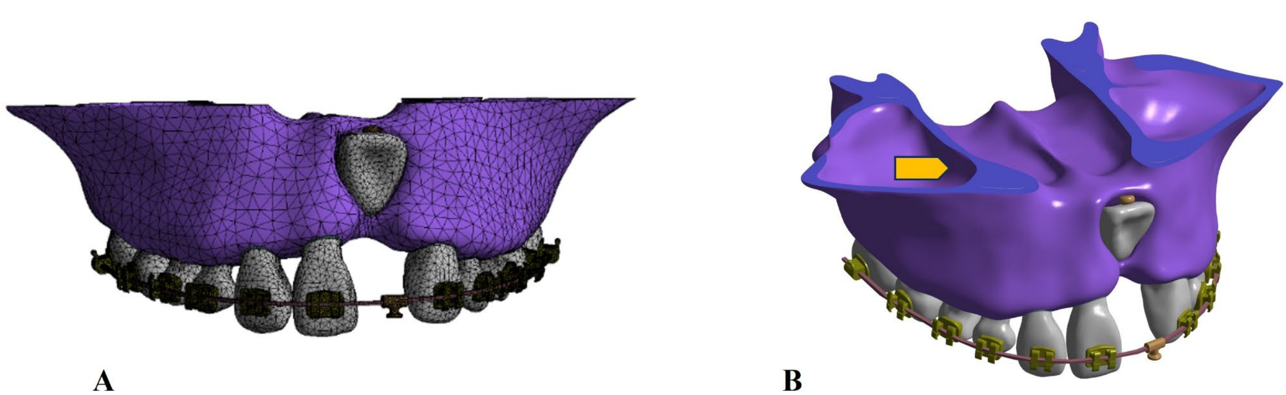

Fig. 2 **A**; Finite element mesh of the impacted dilacerated maxillary central incisor and surrounding structures. **B**; Finite element model illustrating the boundary conditions applied to the maxilla: The upper part of the maxilla was fully constrained in all three directions (x, y , and z) to simulate fixed support, preventing displacement and rotation in all three directions; horizontal (x-axis), sagittal (y -axis), and vertical (z-axis). This constraint was chosen to replicate the anatomical stability of the maxilla during orthodontic traction, ensuring that forces applied to the impacted tooth accurately reflect clinical conditions. Label with yellow color indicates the specific constrained regions

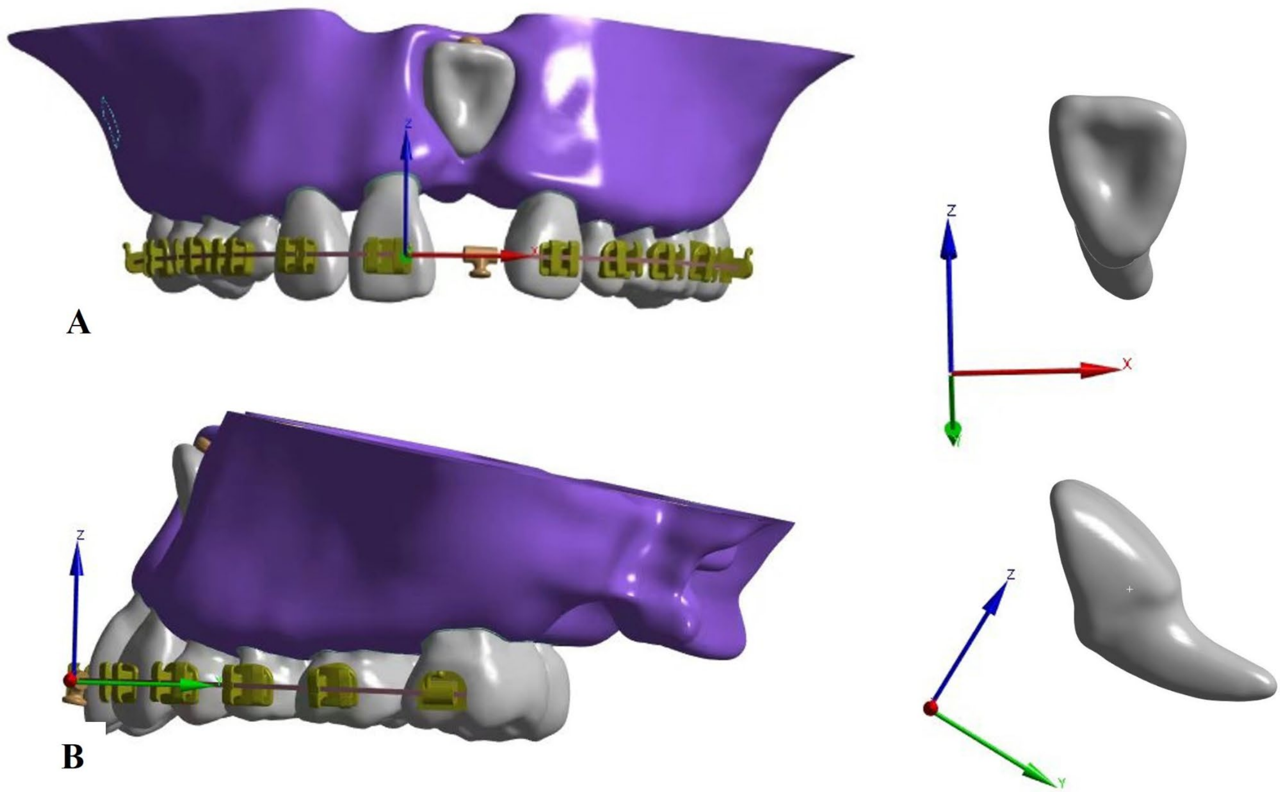

Fig. 3 The coordinate system used for analysis was based on the local coordinate system, with the crown centroid as the reference point. **A**; coronal view, and **B**; sagittal view. The axes were defined as follows: the *x*-axis represented the mesiodistal direction (+ mesial, −distal), the *y*-axis represented the tooth root direction (+ palatal, −labial), and the *z*-axis represented the direction perpendicular to the crown (the incisogingival direction), with gingival as the positive direction and incisal as the negative

direction) represented the positive mesial and the negative distal directions. At the same time, the y-axis (the direction of the tooth root) denoted the positive labial and negative palatal directions. The *z*-axis (perpendicular to the tooth crown) represented the incisogingival direction, with gingival as the positive and incisal as the negative. The upper part of the maxilla's displacement and rotation in the horizontal *x*-axis, sagittal *y*-axis, and vertical *z*-axis directions were all constrained. Additionally, under all conditions, a concentrated traction force of 100 gm was applied in the vertical direction along the long axis of the impacted tooth's crown, and the loading duration for all conditions was 1 s (Fig. 4).

For ease of observation, the software used different colors to represent varying stress distributions, with colors ranging from blue to red indicating increasing stress levels.

Results

3D directional displacement of the impacted tooth

Based on the FEA performed on the four models with varying positions of the orthodontic traction button, the directional displacement of the labially impacted dilacerated maxillary central incisor in the three directions (*x*-axis mesiodistally, *y*-axis labiopalatally, and *z*-axis vertically) was (as shown in Figs. 5): In model A, the displacement was observed to be minimal on the *x*-axis (0.0774 MPa), while was a significant displacement on axes *y*and *z*, 0.0826 MPa, 0.226 MPa, respectively. In model B, there was a notable mesiodistal displacement on the *x*-axis of 0.0718 MPa, while minimal displacement occurred in the labial direction (*y*-axis) of 0.0853 MPa. On the *z*-axis, the vertical displacement was the highest among all models (0.2322 MPa). Regarding model C, on the *x*-axis, moderate mesial displacement was observed (0.0648 MPa), and the displacement in the labiopalatal direction was considerable (0.0745 MPa). On *z*-axis, vertical displacement was moderate (0.1985 MPa). For model D, displacement was significant on the *x*-axis toward the mesial direction (0.0554 MPa) and considerable labial displacement on the *y*-axis (0.0667 MPa). On the *z*-axis was the moderate vertical displacement of the impacted tooth (0.1734 MPa) (See Fig. 6; Table 2).

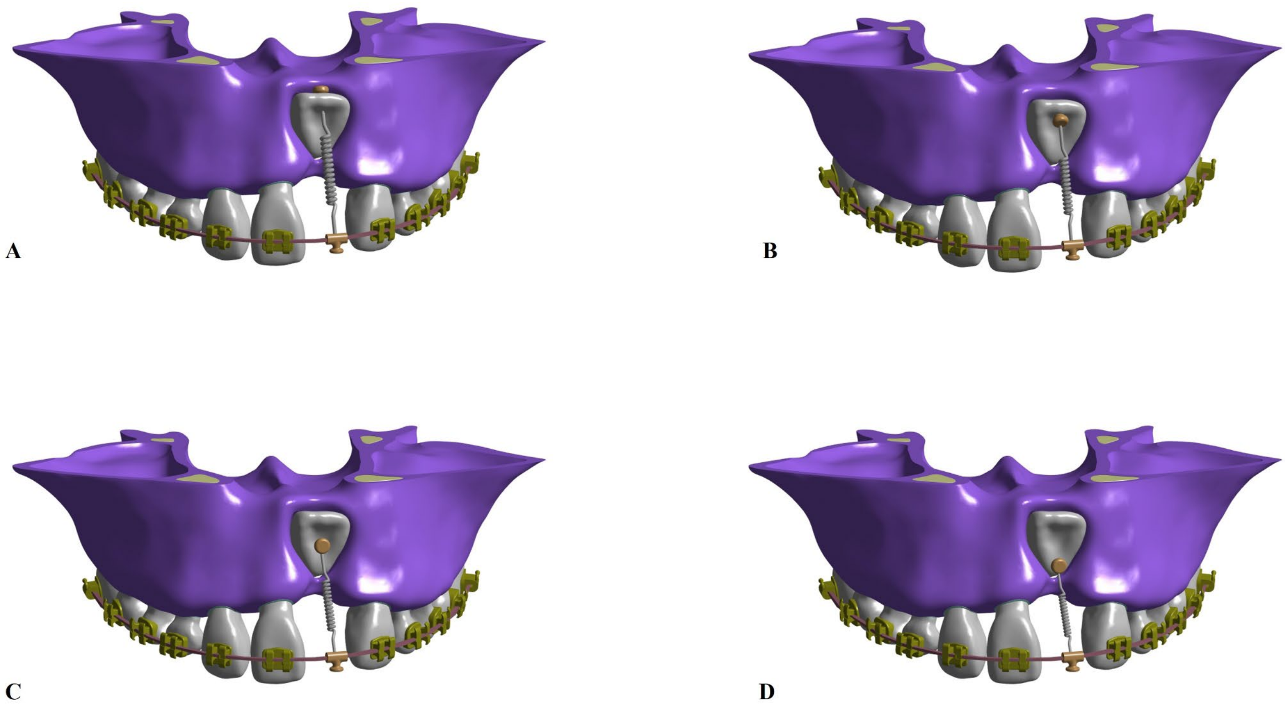

Fig. 4 The load conditions illustrate the application of traction force. In each model, a 100 g traction force was applied vertically along the long axis of the impacted tooth's crown. The point of application was centered mesiodistally, from the traction button on the impacted tooth's crown to the hook on the archwire. The four models (**A**, **B**, **C**, and **D**) represent different positions of the traction button on the labially impacted dilacerated maxillary central incisor: **A**; an incisal third of the labial surface, **B**; an incisal third of the palatal surface, **C**; middle third of the palatal surface, and D; cervical third of the palatal surface

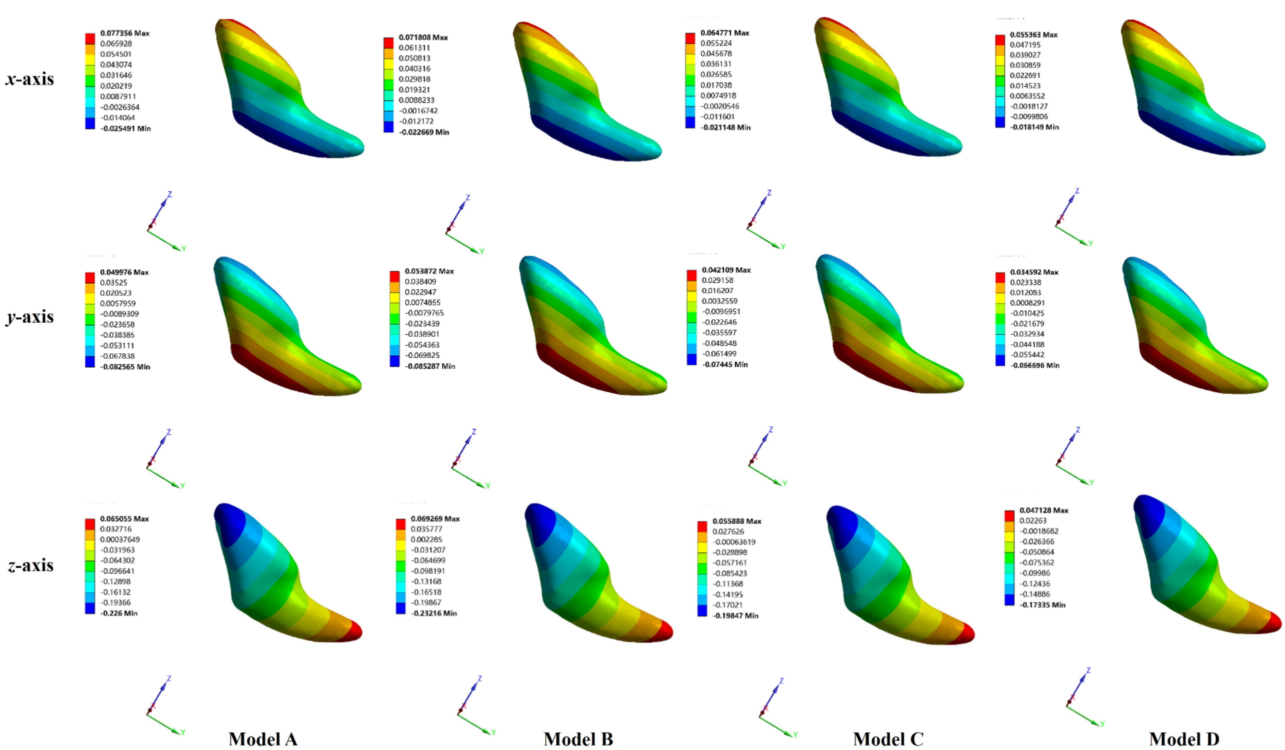

Fig. 5 3D directional displacements of the impacted dilacerated maxillary central incisor. The vector diagrams and color maps showed initial patterns of impacted tooth displacement. The *x*-axis represented the mesiodistal direction (+mesial, −distal), the *y*-axis represented the tooth root direction (+palatal, −labial), and the *z*-axis represented the direction perpendicular to the crown, with gingival as the positive direction and incisal as the negative

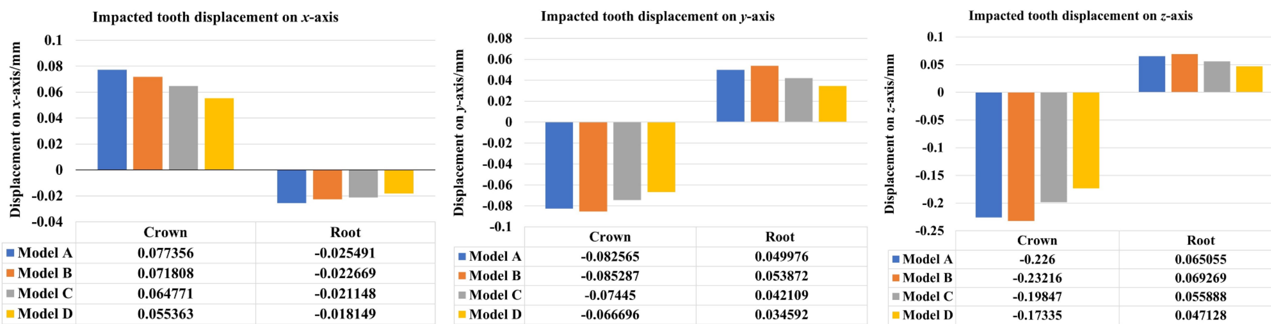

Fig. 6 The bar charts show the 3D directional displacement of the impacted dilacerated maxillary central incisor displayed as crown and root displacement, respectively (in mm) in the *x*, *y* and *z* directions. Model A, Model B, Model C, and Model D. In the *x*-axis (mesiodistal displacement), the maximum displacement was in model A among all models, followed by model B, and the minimum displacement was in model D. In the *y*-axis (labiopalatal displacement), the maximum displacement was in model B among all models followed by model A, and the minimum displacement was in model D. In the *z*-axis (vertical displacement), the maximum displacement was in model B among all models followed by model A, and the minimum displacement was in model D

Table 2 3D directional displacement of impacted dilacerated maxillary central incisor in three directional axes X, y, and Z

	Model A		Model B		Model C		Model D	
	Crown	Root	Crown	Root	Crown	Root	Crown	Root
x-axis	0.077	-0.026	0.072	-0.023	0.065	-0.021	0.055	-0.018
y-axis	-0.083	0.050	-0.085	0.054	-0.075	0.042	-0.067	0.035
z-axis	-0.226	0.065	-0.232	0.069	-0.199	0.056	-0.173	0.047

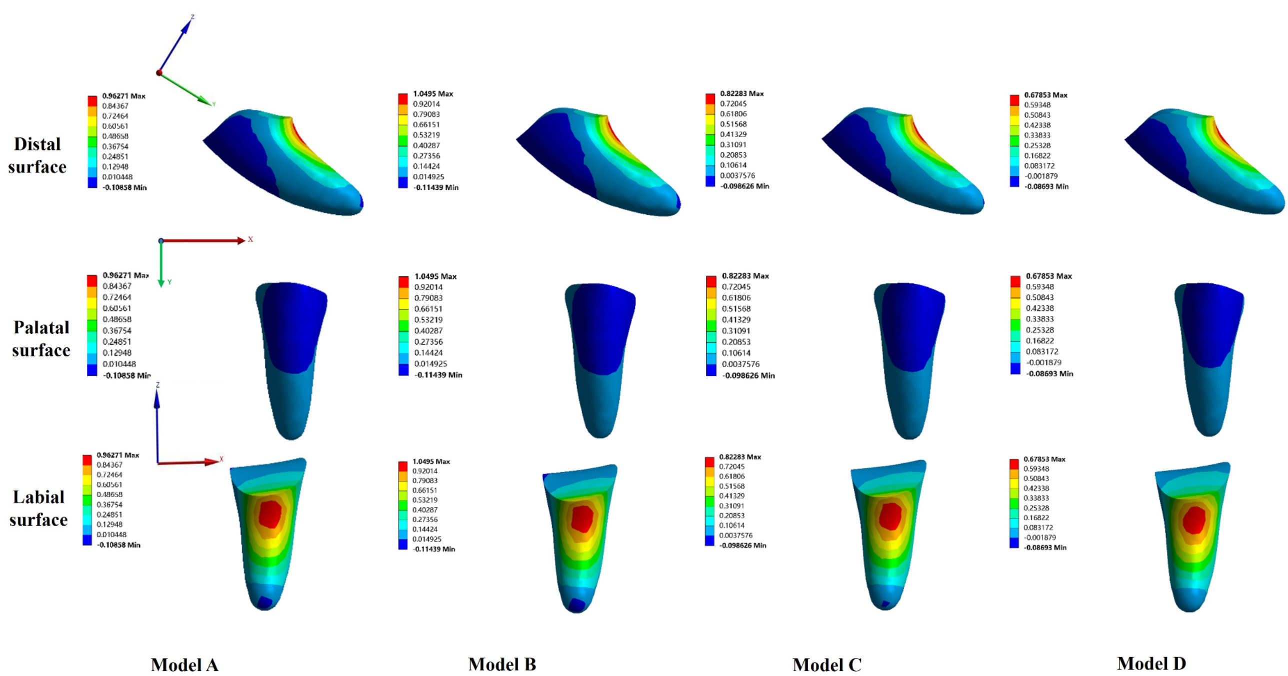

Fig. 7 The stress distribution on the impacted tooth root in MPa. Model A, Model B, Model C, Model D. All models showed the middle cervical regions labially experiencing the highest stresses, which were represented by a gradient from yellow to red on the cervical region labially. Conversely, the middle palatal region and the apical region showed the lowest stress, which was represented by dark blue color

The impacted tooth root stress

The stress distribution characteristics of the impacted tooth root were similar across all models (See Figs. 7 and 8). The stress was primarily concentrated on the labial surface, especially the cervical region. All models indicated that the cervical region consistently experiences the highest stress, while the apical region has the lowest. Model B had the highest stress (1.0495 MPa), and model D had the lowest (0.6785 MPa) (See Table 3).

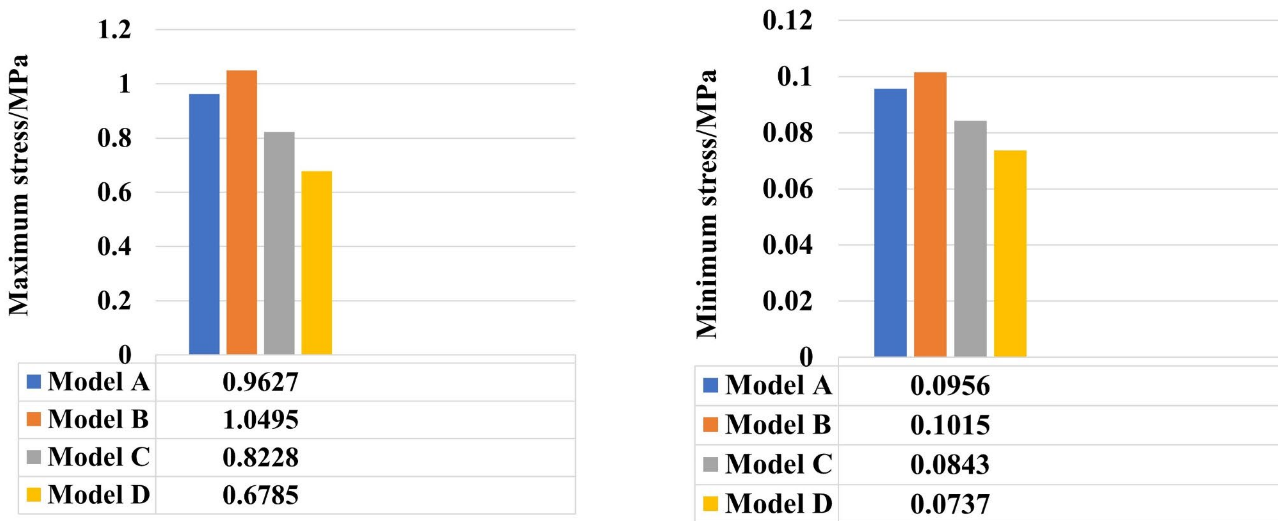

Fig. 8 The bar charts show the stress on the impacted tooth root in MPa. Model A, Model B, Model C, and Model D. Model B had the highest maximum principal stress, followed by model A and then model C. Model D showed the lowest maximum principal stress, indicating a more even stress distribution

Table 3 The comparison of the stress values across models A, B, C, and D

	Model A		Model B		Model C		Model D	
	Maximum stress	Minimum stress	Maximum stress	Minimum stress	Maximum stress	Minimum stress	Maximum stress	Minimum stress
Impacted tooth root stress	0.963	0.096	1.050	0.102	0.823	0.084	0.679	0.074
Alveolar bone Von Mises stress	0.201	-0.031	0.203	-0.039	0.176	-0.032	0.168	-0.024
PDL hydrostatic stress	0.064	-0.116	0.064	-0.122	0.059	-0.105	0.054	-0.094

The alveolar bone Von Mises stress

The alveolar bone Von Mises stress distribution was similar across all models and primarily concentrated on the impacted tooth's palatal surface extending to the adjacent teeth' cervical region (Figs. 9 and 10). The middle palatal cervical region showed higher stress values, while the lower values were near the apical region. Models A and B had comparable Von Mises stresses (0.2016 MPa, 0.2031 MPa), respectively, while model D had the lowest at 0.1676 MPa, and model C displayed a moderate value of 0.1755 MPa (Table 3).

Periodontal ligament hydrostatic stress

The maximum hydrostatic stress (tensile stress) in all models was found in the mesio-labial and apical palatal regions; in contrast, the minimum hydrostatic stress (compressive stress) was located in the palatal cervical region, as illustrated in Figs. 11 and 12. The tensile stress was highest in models A (0.0635 MPa) and B (0.0644 MPa). The compressive stress values exceeded the critical threshold of -0.0047 MPa for external root resorption risk [24, 25]. Model B had the highest compressive stress at -0.1217 MPa, followed by model A at -0.1162 MPa, and model D showed the lowest compressive stress at -0.0937 MPa (Table 3).

Discussion

In orthodontics, a precise understanding of the dynamics of tooth movement precisely forces and moments is essential for effectively addressing the complex challenges posed by impacted maxillary central incisors [13, 26]. These concepts determine how impacted teeth respond to applied orthodontic forces. When dealing with teeth with short roots, the movement dynamics change significantly; the center of resistance shifts apically, leading to an increased moment-to-force (M/F) ratio [27]. This shift can facilitate more controlled root movement but raises concerns about tooth stability and potential adverse effects. A well-placed force can promote effective tooth movement, while improper application may result in undesirable outcomes such as root resorption or instability [28].

By employing FEA, we can simulate and analyze the intricate interactions of forces on impacted teeth. This approach not only enhances our understanding of the biomechanical implications but also aids in developing optimized treatment strategies tailored to the unique anatomical and clinical conditions of impacted incisors. Previous studies have examined the biomechanical aspects of impacted central incisors. Wang et al. [13] examined stress patterns in the periodontal ligament of impacted central incisors. They found that excessive force

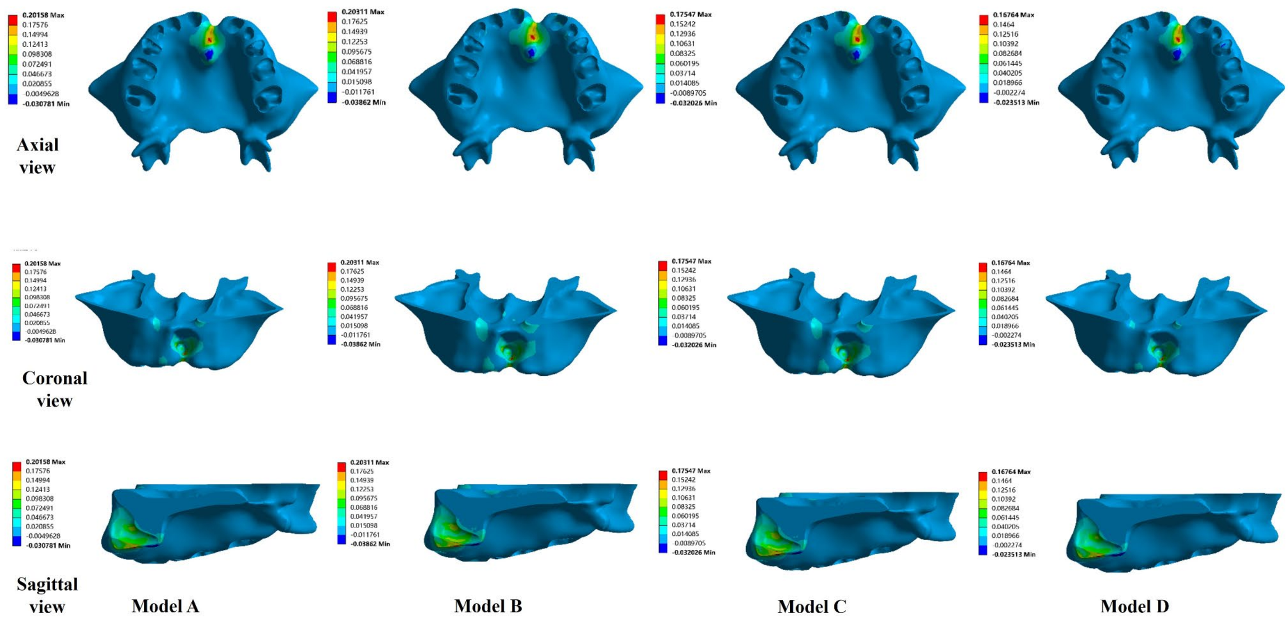

Fig. 9 The distribution of the Von Mises stress of alveolar bone in the impacted tooth area in MPa. The stresses of the alveolar bone were primarily distributed on the palatal surface with a concentration in the middle region. The middle palatal region near the cervical region exhibited a gradient from yellow to red, indicating a higher stress area. In contrast, the palatal region near the apical area was dark blue, suggesting a lower stress area

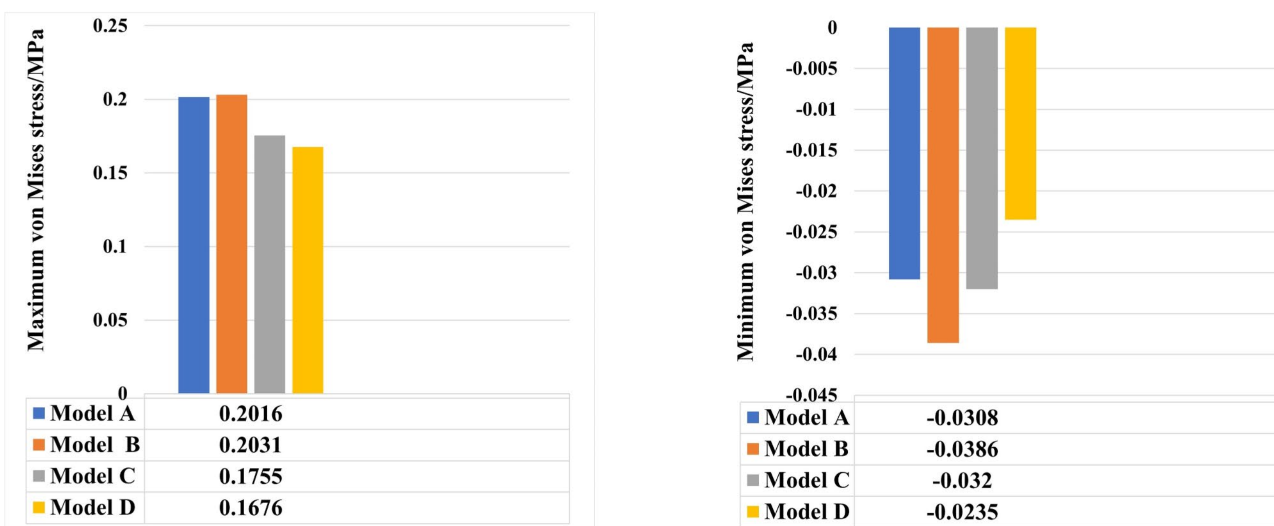

Fig. 10 The bar chart of the Von Mises stress of alveolar bone in the impacted tooth area in MPa. Models A and B showed similar maximum stress with little difference. While, model D showed the lowest maximum principal stress. Model C showed moderate increasing stress

application could result in localized stress concentration, increasing the risk of root resorption. Yang et al. [11] analyzed the effects of different force directions on inverted incisors using FEA. They found that the angle of traction significantly influences stress distribution, recommending angles between 100–120° for optimal results. These findings align with our study regarding the importance of optimizing force direction. So, the previous studies utilizing FEA have provided insights into the stress distribution in periodontal tissues and root structures under different orthodontic traction forces. However, these studies have primarily focused on the overall force application rather than the influence of traction button positioning. Therefore, this study aimed to conduct a biomechanical analysis using 3D FEA on a labially impacted dilacerated maxillary central incisor, focusing on the effects of different positions of the traction button on the tooth crown during orthodontic traction. To our knowledge, this was the first biomechanical study to focus on this aspect and could provide additional insights into the biomechanical effects of traction button placement, an aspect not explicitly addressed in these previous studies.

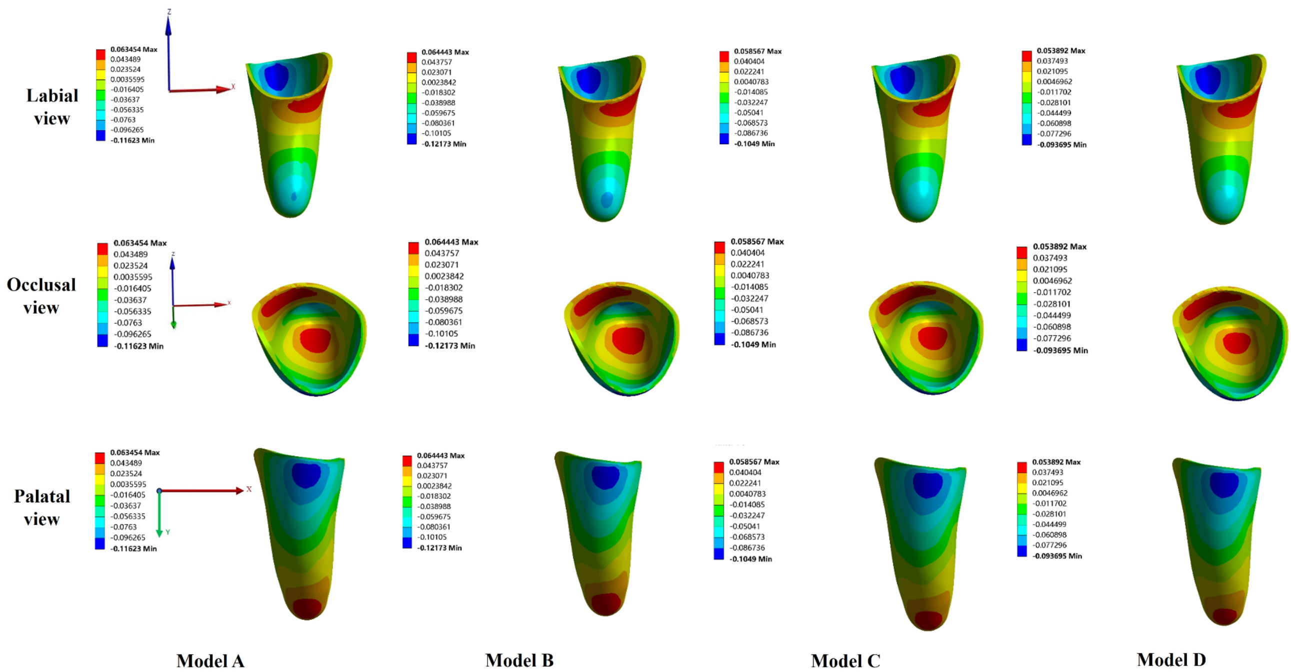

Fig. 11 The distribution of the hydrostatic stress of PDL of the impacted tooth. Positive values indicate tensile stresses for PDL hydrostatic stresses, while negative values indicate compressive stresses. In all four models, the maximum hydrostatic stress was found in the mesio-labial and apical palatal regions that exhibited with dark red color, while the minimum hydrostatic stress was concentrated on the palatal cervical region that exhibited with dark blue color

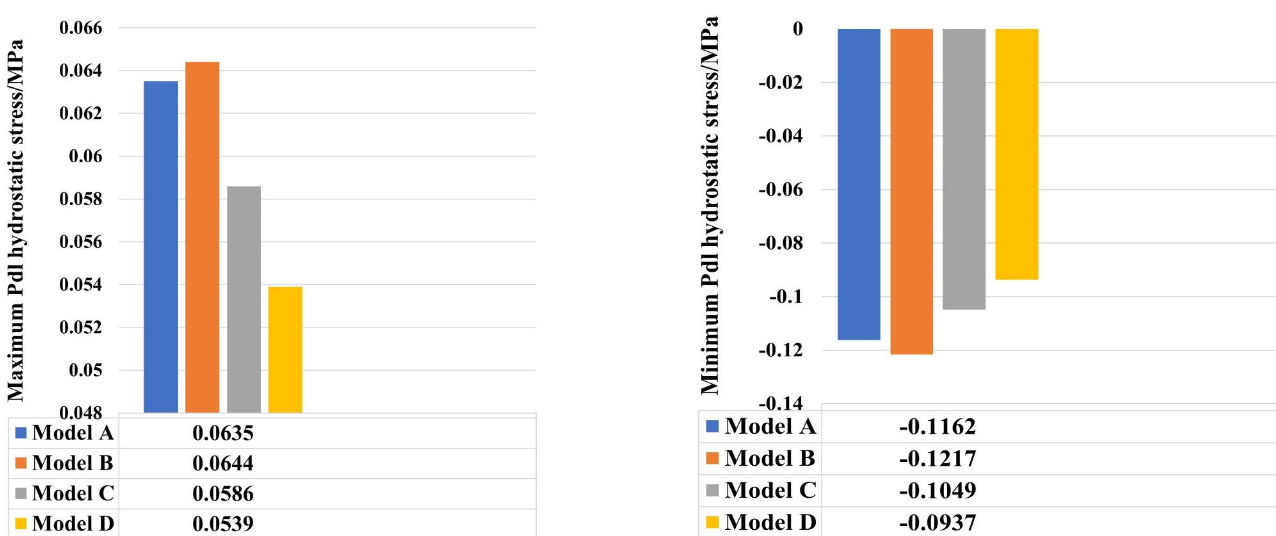

Fig. 12 The bar charts show the hydrostatic stress for PDL of the impacted tooth. Positive values indicate the maximum hydrostatic stress (tensile stresses), while negative values indicate the minimum hydrostatic stress (compressive stress)

Bishara et al. [29] emphasized the importance of button positioning for effective tooth movement, highlighting that improper placement could lead to undesired movement patterns. The current study demonstrated that different button positions resulted in varied tooth displacement patterns. For example, model A and model B, with varying button placements, exhibited significant differences in mesiodistal and vertical movements, underscoring the critical role of button positioning in achieving desired orthodontic outcomes. The force direction in traction influences displacement and the stress exerted on surrounding alveolar structures, which has been previously confirmed in clinical research [30]. In the model with the traction button placed on the incisal third of the labial surface, the displacement along the x-axis was minimal, indicating limited movement in the mesial direction; however, its mesial displacement was the highest among all models. Significant displacement was also along the *y* and *z* axes, indicating effective labial movement and efficient extrusion. In the model with the traction button on the incisal third of the palatal surface, the labial (y-axis) and vertical (z-axis) displacements were the highest among all models, indicating the most effective labiopalatal displacement and extrusion. In models A and B, the traction button's placement at a considerable distance from the center of resistance produced a large momentum, resulting in significant displacements [31]. Conversely, the button's position on the cervical third of the palatal surface resulted in the least movement in all directions compared to the other models. In this configuration, the button was closer to the center of resistance, which produced less momentum, so the displacement of the tooth was limited. Additionally, the displacement magnitudes and directions predicted by our model are consistent with established orthodontic biomechanics principles [32, 33]. Specifically, the labiopalatal and vertical displacements observed in model B, which showed the highest displacement among all models, were in agreement with previous findings on force application during traction of impacted incisors.

A previous study using FEA to simulate a three-dimensional model of a human maxillary central incisor subject to various orthodontic force types reported that a tooth with a longer root incurs more mechanical stress at the apex than a shorter one of the same size [34]. This was interpreted as the longer root having more cementum increments, increasing mechanical stress [34]. Clinically, longer teeth have been found to have more root resorption [35]. This was in line with the current study's findings on the labially impacted dilacerated maxillary central incisor with a short root. The cervical region showed the highest stresses across all placements in all models, while the apex had the lowest. The stress distribution was mainly located on the labial and palatal surfaces, concentrating on the cervical and middle regions. Excessive stress concentrations in these areas can contribute to root resorption, as demonstrated in a recent study of finite element analysis of orthodontic traction [24].

The traction button on the incisal third of the palatal surface showed the highest stresses, highlighting the need for careful traction force management to avoid excessive stress concentrations. Iwasaki et al. [32] and Proffit et al. [33] emphasized the importance of stress concentrations in the cervical region for tooth movement and periodontal health. Conversely, the traction button on the cervical third of the palatal surface exhibited the lowest stresses, indicating a more favourable stress distribution for orthodontic applications. A notable agreement was observed in stress concentration patterns. Similar to previous studies [11, 13, 14], our study confirmed that stress is highest in the cervical region of the impacted tooth and that excessive stress in this area could contribute to root resorption. However, our results extend these findings by demonstrating how different traction button placements influence the magnitude and distribution of these stresses. The button's placement on the incisal third of the palatal surface (model B) resulted in the highest root stress.

In contrast, the button on the cervical third of the palatal surface (model D) minimized stress concentrations. These results suggest that proper button positioning could be a clinical strategy to balance efficient tooth movement with the risk of adverse effects. The consistent high stress in the cervical area rather than the root apex suggests a reduced likelihood of root resorption, particularly since impacted dilacerated teeth generally have shorter roots, resulting in less mechanical stress at the apex. Therefore, the root resorption rate would be lower, which aligned with the findings of previous studies [34, 35]. However, continuous monitoring and adjustments based on individual stress distributions are essential to ensure the long-term health of the periodontal tissue.

The traction process of labially impacted dilacerated maxillary central incisor can increase the risk of palatal alveolar bone loss and result in root resorption [11, 30, 36]. The current study found a slight variation in the stress exerted on the alveolar bone surrounding the root due to various positions of the traction button. In all models, the highest Von Mises stress in the alveolar bone typically appeared on the palatal surface and extended into the cervical regions of adjacent teeth. The middle palatal region near the cervical area, crucial for tooth stability, exhibited higher stress values, indicating significant stress concentrations. Clinical studies have reported similar findings evaluating long-term orthodontic traction effects on alveolar bone integrity [37]. The traction button positioned on the incisal third of the labial or palatal surface experienced the highest alveolar bone stress levels. These findings suggested that these two button positions are subjected to higher traction forces, which could lead to adverse effects such as microdamage, bone resorption, fenestration, or even dehiscence over time. This was supported by research from Furlan et al. [37], which identified differences in stress in the alveolar bone tissue based on various orthodontic forces, suggesting the potential for dehiscence or fenestration.

While Furlan et al. reported stress distribution in the alveolar bone under different orthodontic forces, our study highlighted how traction button placement influences stress levels in specific regions. Our findings showed that button placements closer to the incisal third (models A and B) resulted in higher Von Mises stress in the alveolar bone, particularly on the palatal surface. This suggested a greater risk of alveolar bone resorption, which was not explicitly detailed in previous studies. In contrast, the button on the cervical third of the palatal surface exhibited the lowest stress, indicating a more favourable stress distribution, potentially reducing the risk of damage to the alveolar bone.

The higher stress concentrations observed in models A and B, particularly in the palatal surface of the alveolar bone, suggested an increased risk of long-term biological effects. Prolonged exposure to high-stress levels in the PDL might lead to vascular compression, reduced blood flow, and potential tissue necrosis, ultimately contributing to root resorption. Additionally, sustained high stress in the alveolar bone could trigger bone remodeling imbalance, increasing the risk of localized bone resorption, fenestration, or dehiscence over time. These risks align with previous clinical findings indicating that excessive orthodontic forces could lead to adverse periodontal outcomes [32, 33]. In contrast, Model D, which exhibited the lowest stress concentrations, might reduce these risks but result in slower tooth movement due to lower force efficiency. Therefore, a balanced approach in selecting the optimal traction button position is essential to achieve effective tooth movement while minimizing periodontal and alveolar bone damage.

The insufficient force applied to the PDL would not elicit periodontal tissue reaction, or the reaction efficiency would be too minimal [24, 25]. Conversely, excessive force could cause harm to the PDL, leading to root resorption. It was suggested that if the PDL hydrostatic stress exceeds the capillary pressure in the area, the vessels would collapse, and blood flow to that area would be impaired, increasing the risk of root resorption. As reported by previous investigations [24], the threshold for capillary pressure in the PDL was estimated to be >0.0047 MPa, which represented a substantial growth of the risk of external root resorption [12, 24, 25]. The current study found that the tensile stresses on the PDL were mainly concentrated on the mesio-labial cervical and apical palatal regions. In contrast, the compressive stress for all models was located on the cervical region palatally. Similarly, the hydrostatic stress values in the periodontal ligament followed trends reported by Jifang et al. [14], who analyzed stress patterns during orthodontic traction. The traction button on the incisal third of the palatal surface exhibited the highest stresses, followed closely by the button on the incisal third of the labial surface. In contrast, the button on the cervical third of the palatal surface had the lowest, indicating a reduced risk of root resorption. These stress distributions indicated areas prone to micro-damage, potentially affecting the integrity of the PDL [32, 38, 39]. Previous clinical investigations have also highlighted the need to optimize orthodontic force magnitude to prevent excessive PDL stress and related complications [32]. The variations in hydrostatic stress underscored the necessity of personalized treatment planning [32, 33]. The compressive stress of -0.1217 MPa observed in the periodontal ligament in our model fell over the range reported for capillary pressure in the periodontal microcirculation, typically around 0.0047 MPa and 0.016 MPa. The exceeded compressive stresses could reduce blood flow tissue ischemia, leading to root resorption and potential damage to the alveolar bone [40]. The −0.1217 MPa compressive stress in our study suggested that under certain conditions, excessive compressive forces could contribute to root and alveolar bone resorption, especially in the presence of other risk factors such as inflammation, poor bone support, or prolonged or excessive forces or improper force application. Additionally, Moga et al. [41] further corroborated these findings, indicating that compressive forces near capillary pressure levels were particularly risky for periodontal health. Understanding these biomechanical responses enables clinicians to tailor their approaches, reducing risks and enhancing patient outcomes. Also, the clinical application of these findings depends on individual patient conditions. In cases where the patient has preexisted alveolar bone loss, a thin periodontal ligament, or a history of root resorption, minimizing stress on the PDL and alveolar structures becomes a higher priority, making a more cervical traction button position (e.g., model D) preferable despite slower tooth movement. Conversely, in patients with thicker PDL, adequate bone support, and a need for faster traction to align the incisor within a limited timeframe, a more incisal traction position (e.g., models A or B) may be clinically justified, provided that forces are carefully monitored to avoid excessive stress-related complications. This trade-off highlights the importance of individualized treatment planning to balance biomechanical efficiency with periodontal safety.

The results presented in this study were based on the initial displacement of the tooth following force application. Since orthodontic tooth movement is a dynamic process influenced by biological remodelling and long-term mechanical interactions, these findings should be interpreted within the context of early-stage movement. Future studies incorporating time-dependent (4D) analysis would be beneficial in understanding the whole progression of orthodontic treatment.

Limitation

While the findings of this study provide valuable insights into the biomechanics of orthodontic traction for labially impacted dilacerated maxillary central incisors, several limitations should be acknowledged. First, material properties were simplified for computational feasibility. The PDL was modelled as a uniform linear elastic material, whereas, in reality, it exhibits nonlinear viscoelastic behaviour with variable thickness across different regions. This simplification may influence stress distribution, particularly in the PDL and surrounding structures. Future studies should consider incorporating more physiologically accurate material models to better simulate periodontal tissue response under orthodontic forces. Second, this study utilized a static FEA, meaning that the effects of dynamic loading conditions, such as cyclic orthodontic forces and masticatory loads, were not considered. In clinical settings, orthodontic forces fluctuate over time due to patient-specific functional movements and force decay from orthodontic appliances. Future studies should integrate dynamic or time-dependent loading scenarios to represent real-world orthodontic biomechanics better. Third, this study did not account for biological remodelling over time. Orthodontic forces induce gradual changes in bone and periodontal ligament structures through remodelling. However, our simulation only represented the initial mechanical response of the impacted tooth to applied forces. Time-dependent (4D FEA) models would provide a more comprehensive understanding of stress adaptation and tooth movement over time. Lastly, the study was based on a single patient-specific model, which may limit the generalizability of the findings. Anatomical variations, including root morphology, bone density, and periodontal ligament characteristics, can influence the mechanical response to traction.

Additionally, interpatient variability in treatment outcomes due to biological and biomechanical differences has not been accounted for. Future research should incorporate multi-patient models derived from multiple CBCT scans to capture a broader range of clinical scenarios and enhance applicability. The robustness of our findings depended on key factors such as traction force magnitude, material property assumptions, and PDL thickness variations. While the PDL was modelled as a uniform linear elastic material, it exhibits nonlinear viscoelastic behaviour in reality. Additionally, the applied 100 g traction force fell within clinically recommended ranges, and minor variations in force magnitude were unlikely to alter overall stress distribution and displacement trends. Future studies could further quantify these effects through a detailed sensitivity analysis. Despite these limitations, this study provided a foundational analysis of traction button positioning using 3D FEA and offered a valuable reference for optimizing orthodontic treatment strategies for impacted dilacerated maxillary central incisors.

Conclusion

This study underscored the significance of traction button positioning in balancing effective tooth movement with minimizing stress-related complications in the orthodontic traction of labially impacted dilacerated maxillary central incisors:

1. Maximal Tooth Movement vs. Stress Concentration: The traction button on the incisal third of the labial or palatal surface (Models A and B) facilitated significant displacement, particularly in the labiopalatal and vertical directions. However, these placements also resulted in higher stress concentrations in the root, PDL, and alveolar bone, increasing the risk of root resorption and alveolar bone loss.
2. Balanced Approach: The middle third of the palatal surface (Model C) offered a moderate compromise between movement and stress, reducing excessive force transmission while maintaining effective displacement.
3. Minimized Stress for Structural Preservation: The traction button on the cervical third of the palatal surface (Model D) resulted in the lowest stress concentrations in the root, PDL, and alveolar bone, which may be beneficial in cases where preserving structural integrity is paramount. While this placement may slow tooth movement, it provides a safer biomechanical environment, particularly for cases with pre-existing periodontal vulnerability.

Clinical implications

The alignment between our findings and previous studies reinforces fundamental orthodontic biomechanics principles, such as the importance of force magnitude and direction in determining stress distribution. However, the discrepancies regarding traction button positioning indicated that additional clinical considerations are required when selecting optimal traction strategies. For cases requiring faster movement, placing the traction button on the incisal third of the labial or palatal surface (Models A and B) may be effective but necessitates careful monitoring to avoid excessive root and bone stress. For cases with a high risk of root resorption or alveolar bone loss, a more cervical button placement (Model D) may be preferable, even if it results in slower movement. For moderate balance between movement and stress minimization, placing the button in the middle third of the palatal surface (Model C) is a reasonable compromise.

Abbreviations

FEA	Finite element analysis
FEM	Finite element model
3D	Three-dimensional
PDL	Periodontal ligament
CBCT	Cone-beam computed tomography
STL	Stereolithography or Standard Tessellation Language
DICOM	Digital Imaging and Communication in Medicine
NX software	Next generation software
MPa	Megapascal

Acknowledgements

Not applicable.

Author contributions
E.S.A.: Software, Validation, Methodology, Data collection and analysis, Writing-original draft. B.W.Z.: Writing review and editing, Conceptualization, Supervision. W.T.: Conceptualization, Methodology, Validation, Investigation. M.Y.L.: Methodology, Data analysis. H.P.W.: Methodology and Data curation. X.F.Y., B.S.A., N.A.A., M.A.A.A., and M.S.A.: Methodology, Validation, Data curation. Y.L.: Methodology, Resources, Conceptualization, Supervision.

Funding
This work was supported by Basic Scientific Research Project of Education Department of Liaoning Province (LJKMZ20221190) and Liaoning Province Doctoral Research Start-up Fund project (2022-BS-150).

Data availability
The data supporting the findings of this study are available from the corresponding author upon reasonable request.

Declarations

Ethics approval and consent to participate
This study was approved by the ethical committee of clinical scientific research of China Medical University and Stomatology Hospital of China Medical University, China, Ethics Approval Number: (No. K-2024-018). Informed written consent was obtained from the participant's parents before the patient entered the study. All methods were carried out in accordance with the principles of the Declaration of Helsinki.

Consent for publication
Not applicable.

Competing interests
The authors declare no competing interests.

Author details
[1]Department of Orthodontics, School and Hospital of Stomatology, Liaoning Provincial Key Laboratory of Oral Disease, China Medical University, Shenyang, Liaoning 110002, China
[2]Shenyang Clinical Medical Research Center of Orthodontic Disease, Shenyang, Liaoning 110002, China
[3]Department of Orthodontics and Dentofacial Orthopedics, Faculty of Dentistry, Ibb University, IBB, Yemen
[4]Department of Oral and Maxillofacial Surgery, Faculty of Dentistry, Thamar University, Thamar, Yemen
[5]Department of Orthodontics, Ningbo Dental Hospital, Ningbo, Zhejiang 315032, China
[6]Orthodontics Division, Faculty of Medicine and Health Sciences, Taiz University, Taiz, Yemen
[7]Orthodontics and Dentofacial Orthopedics, Department of Preventive Dental Sciences, College of Dentistry, Jazan University, Jazan, Saudi Arabia

Received: 4 February 2025 / Accepted: 7 April 2025
Published online: 22 May 2025

References

1. Pavoni C, Mucedero M, Laganà G, Paoloni V, Cozza P. Impacted maxillary incisors: diagnosis and predictive measurements. Ann Stomatol (Roma). 2012;3(3–4):100–5.
2. Mockutė G, Klimaitė G, Smailienė D. The morphology of impacted maxillary central incisors: A systematic review. Med (Kaunas) 2022, 58(4).
3. Seehra J, Yaqoob O, Patel S, O'Neill J, Bryant C, Noar J, Morris D, Cobourne MT. National clinical guidelines for the management of unerupted maxillary incisors in children. Br Dent J. 2018;224(10):779–85.
4. Lygidakis NN, Chatzidimitriou K, Theologie-Lygidakis N, Lygidakis NA. Evaluation of a treatment protocol for unerupted maxillary central incisors: retrospective clinical study of 46 children. Eur Arch Paediatr Dent. 2015;16(2):153–64.
5. Wu G, He S, Chi J, Sun H, Ye H, Bhikoo C, Du W, Pan W, Voliere G, Hu R. The differences of root morphology and root length between different types of impacted maxillary central incisors: A retrospective cone-beam computed tomography study. Am J Orthod Dentofac Orthop. 2022;161(4):548–56.
6. Du W, Chi J, He S, Wu G, Pan W, Wang Y, Voliere G, Hu R. The position and morphology characteristics of multiple impacted anterior teeth in the unilateral maxillary area: A retrospective study based on cone-beam computed tomography. Am J Orthod Dentofac Orthop. 2022;162(6):907–16.
7. Huber KL, Suri L, Taneja P. Eruption disturbances of the maxillary incisors: a literature review. J Clin Pediatr Dent. 2008;32(3):221–30.
8. de Amorim CS, Americano GCA, Moliterno LFM, de Marsillac MWS, Andrade MRTC, Campos V. Frequency of crown and root dilaceration of permanent incisors after dental trauma to their predecessor teeth. Dent Traumatol. 2018;34(6):401–5.
9. Lin YT. Treatment of an impacted dilacerated maxillary central incisor. Am J Orthod Dentofac Orthop. 1999;115(4):406–9.
10. Gupta SP, Giri J, Shrestha BK. An Orthodontic Approach for the Correction of Transposition along with Multiple Impacted Teeth. *Case Rep Dent* 2023, 2023:6252389.
11. Yang Q, Yang L, Li N, Sun K, Li L, Wang Y, Han X, Wang T. Effect of force direction and impaction angulation during dilaceration impacted central incisor traction: a finite element analysis. BMC Oral Health. 2024;24(1):823.
12. Liu X, Cheng Y, Qin W, Fang S, Wang W, Ma Y, Jin Z. Effects of upper-molar distalization using clear aligners in combination with class II elastics: a three-dimensional finite element analysis. BMC Oral Health. 2022;22(1):546.
13. 王勤波. 王玲, 刘又南, 刘振田: 埋伏倒置上中切牙导萌正畸中旋转中心变化规律的研究. 实用口腔医学杂志. 2004;20(2):204–6.
14. Jifang H, Han Z, Xiaodong Q, Weijun Y, Ping S. [Finite element analysis of periodontal tissue stress distribution of labial inverted impacted maxillary central incisor]. Hua Xi Kou Qiang Yi Xue Za Zhi. 2015;33(1):67–70.
15. Ouldyerou A, Mamboleo E, Gilchrist L, Alsharif K, Ngan P, Merdji A, Mukdadi O. In-silico evaluation of orthodontic miniscrew-assisted rapid palatal expanders for patients with various stages of skeletal maturation. Am J Orthod Dentofac Orthop. 2024;166(6):561–71.
16. Kapila S, Sachdeva R. Mechanical properties and clinical applications of orthodontic wires. Am J Orthod Dentofac Orthop. 1989;96(2):100–9.
17. Ma Y, Li S. The optimal orthodontic displacement of clear aligner for mild, moderate and severe periodontal conditions: an in vitro study in a periodontally compromised individual using the finite element model. BMC Oral Health. 2021;21(1):109.
18. Gomez JP, Peña FM, Martínez V, Giraldo DC, Cardona CI. Initial force systems during bodily tooth movement with plastic aligners and composite attachments: A three-dimensional finite element analysis. Angle Orthod. 2015;85(3):454–60.
19. Ammar HH, Ngan P, Crout RJ, Mucino VH, Mukdadi OM. Three-dimensional modeling and finite element analysis in treatment planning for orthodontic tooth movement. Am J Orthod Dentofac Orthop. 2011;139(1):e59–71.
20. Cheng Y, Gao J, Fang S, Wang W, Ma Y, Jin Z. Torque movement of the upper anterior teeth using a clear aligner in cases of extraction: a finite element study. Prog Orthod. 2022;23(1):26.
21. Ouldyerou A, Ngan P, Alsharif K, Merdji A, Mukdadi OM. Biomechanical performance of ATOZ expander: Finite-element analysis. Am J Orthod Dentofac Orthop. 2025;167(3):331–44.
22. Shalish M, Cooper-Kazaz R, Ivgi I, Canetti L, Tsur B, Bachar E, Chaushu S. Adult patients' adjustability to orthodontic appliances. Part I: a comparison between labial, lingual, and invisalign™. Eur J Orthod. 2011;34(6):724–30.
23. Mamboleo E, Ouldyerou A, Alsharif K, Ngan P, Merdji A, Roy S, Mukdadi OM. Biomechanical analysis of orthodontic Miniscrew-Assisted rapid palatal expansion on dental and bone tissues: A Finite-Element study. J Eng Sci Med Diagnostics Therapy 2024, 7(4).
24. Hohmann A, Wolfram U, Geiger M, Boryor A, Sander C, Faltin R, Faltin K, Sander FG. Periodontal ligament hydrostatic pressure with areas of root resorption after application of a continuous torque moment. Angle Orthod. 2007;77(4):653–9.
25. Dorow C, Sander FG. Development of a model for the simulation of orthodontic load on lower first premolars using the finite element method. J Orofac Orthop. 2005;66(3):208–18.
26. Jacobson A. Biomechanics in orthodontics: principles and practice. Am J Orthod Dentofac Orthop. 2011;139(1):139–40.
27. Choy K, Pae EK, Park Y, Kim KH, Burstone CJ. Effect of root and bone morphology on the stress distribution in the periodontal ligament. Am J Orthod Dentofac Orthop. 2000;117(1):98–105.
28. Kuruthukulam RM, Patil AS. The center of resistance of a tooth: a review of the literature. Biophys Rev Vol. 2023;15:35–41.

29. Bishara SE. Clinical management of impactedmaxillary canines. Semin Orthod. 1998;4(2):87–98.
30. Sun H, Hu R, Ren M, Lin Y, Wang X, Sun C, Wang Y. The treatment timing of labial inversely impacted maxillary central incisors: A prospective study. Angle Orthod. 2016;86(5):768–74.
31. Oh S, Choi Y-K, Kim Y-I, Kim S-S, Park S-B, Kim S-H. The center of resistance of an impacted maxillary canine: A finite element analysis. Appl Sci. 2023;13(20):11256.
32. Iwasaki LR, Haack JE, Nickel JC, Morton J. Human tooth movement in response to continuous stress of low magnitude. Am J Orthod Dentofac Orthop. 2000;117(2):175–83.
33. Proffit WR, Fields HW. Contemporary Orthodontics: Elsevier/Mosby; 2013.
34. Shaw AM, Sameshima GT, Vu HV. Mechanical stress generated by orthodontic forces on apical root cementum: a finite element model. Orthod Craniofac Res. 2004;7(2):98–107.
35. Sameshima GT, Sinclair PM. Predicting and preventing root resorption: part I. Diagnostic factors. Am J Orthod Dentofac Orthop. 2001;119(5):505–10.
36. Sun H, Wang Y, Sun C, Ye Q, Dai W, Wang X, Xu Q, Pan S, Hu R. Root morphology and development of labial inversely impacted maxillary central incisors in the mixed dentition: A retrospective cone-beam computed tomography study. Am J Orthod Dentofac Orthop. 2014;146:709–16.
37. Furlan CC, Freire AR, Ferreira-Pileggi BC, Prado FB, Rossi AC. Fenestration and dehiscence in human maxillary alveolar bone: an in Silico study using the finite element method. Cureus. 2023;15(12):e50772.
38. Li Y, Zhan Q, Bao M, Yi J, Li Y. Biomechanical and biological responses of periodontium in orthodontic tooth movement: up-date in a new decade. Int J Oral Sci. 2021;13(1):20.
39. Hemanth M, Deoli S, Raghuveer HP, Rani MS, Hegde C, Vedavathi B. Stress induced in the periodontal ligament under orthodontic loading (Part I): A finite element method study using linear analysis. J Int Oral Health. 2015;7(8):129–33.
40. Nazeri A, Castillo JA, Ghaffari-Rafi A. Impact of molar distalization with clear aligners on periodontal ligament stress and root resorption risk: A systematic review of 3D finite element analysis studies. Dentistry J. 2025;13(2):65.
41. Moga RA, Buru SM, Chiorean CG, Cosgarea R. Compressive stress in periodontal ligament under orthodontic movements during periodontal breakdown. Am J Orthod Dentofac Orthop. 2021;159(3):e291–9.

Publisher's note